crystals

MDPI

Article

Piezoelectric Properties and Thermal Stability of $Pb(Yb_{1/2}Nb_{1/2})O_3$-$BiScO_3$-$PbTiO_3$ Ternary Ceramics

Fan Zhang [1], Hua Hao [1,2], Minghe Cao [1], Zhonghua Yao [1], Shuai Fu [1] and Hanxing Liu [1,*]

[1] State Key Laboratory of Advanced Technology for Materials Synthesis and Processing, Wuhan University of Technology, Wuhan 430070, China; 269185@whut.edu.cn (F.Z.); haohua@whut.edu.cn (H.H.); caominghe@whut.edu.cn (M.C.); yaozhhua@whut.edu.cn (Z.Y.); intermat@whut.edu.cn (S.F.)

[2] Foshan Xianhu Laboratory of the Advanced Energy Science and Technology Guangdong Laboratory, Xianhu Hydrogen Valley, Foshan 528200, China

* Correspondence: lhxhp@whut.edu.cn

Abstract: Piezoelectric ceramics with excellent piezoelectric properties and a high Curie temperature are important for numerous electromechanical devices in a broad range of temperature environments. In this work, the relaxor ferroelectric $Pb(Yb_{1/2}Nb_{1/2})O_3$ end member was selected to be introduced into a $BiScO_3$-$PbTiO_3$ high-temperature piezoelectric ceramic to reduce the dielectric loss and improve the piezoelectric properties while slightly reducing the Curie temperature. The phase structure and dielectric, ferroelectric and piezoelectric properties of $0.025Pb(Yb_{1/2}Nb_{1/2})O_3$-$(0.975-x)BiScO_3$-$xPbTiO_3$ ($0.60 \leq x \leq 0.63$) ceramics were systematically analyzed, and the best electrical properties were observed in the morphotropic phase boundary region $x = 0.61$ with $d_{33} = 370$ pC/N, $k_p = 44\%$, $P_r = 33.9$ μC/cm^2. Importantly, no significant depolarization was observed in the $x = 0.61$ ceramic from room temperature to 290 °C, demonstrating its good thermal stability and potential applications in a wide range of temperature environments.

Keywords: piezoelectric; high temperature; capacitor; stability

check for updates

Citation: Zhang, F.; Hao, H.; Cao, M.; Yao, Z.; Fu, S.; Liu, H. Piezoelectric Properties and Thermal Stability of $Pb(Yb_{1/2}Nb_{1/2})O_3$-$BiScO_3$-$PbTiO_3$ Ternary Ceramics. *Crystals* **2024**, *14*, 91. https://doi.org/10.3390/cryst14010091

Academic Editor: Maria Gazda

Received: 19 December 2023
Revised: 12 January 2024
Accepted: 17 January 2024
Published: 19 January 2024

1. Introduction

Piezoelectric ceramics, which can convert mechanical energy and electrical energy, are widely used in electronic communication, mechanical manufacturing, military applications and other fields [1–3]. In general, the application temperature range of piezoelectric ceramics is limited to less than half of the Curie temperature due to the depolarization effect during the heating process. For commercial lead zirconate-titanate($Pb(Zr,Ti)O_3$, PZT) piezoceramics, which are widely applied, the Curie temperature is usually lower that 300 °C [4]. In recent years, with the rapid development of energy exploration, vehicle manufacturing, the aerospace industry and other fields, piezoelectric materials have increasingly been required to maintain a stable working state in many harsh environments [5]. For example, the electric injection device of an automobile's internal combustion engine requires piezoelectric materials to work stably in a high-temperature environment above 200 °C or even 300 °C. In the process of petroleum prospecting, piezoelectric sensors for detecting oil pressure and other parameters in deep wells also pose new challenges for the use of piezoelectric materials. Therefore, the development of piezoelectric ceramics with a Curie temperature above 300 °C and excellent piezoelectric properties has become an urgent need to address the demand of growing industrial production [6].

In 2001, Eitel et al. reported a bismuth-based piezoelectric ceramic solid solution with the general formula $Bi(Me)O_3$-$PbTiO_3$, where Me represents ions or ionic groups with a +3 valence state, such as Sc^{3+}, In^{3+}, Yb^{3+}, etc. [7]. Among them, $BiScO_3$-$PbTiO_3$ (BS-PT) piezoelectric ceramics are the most significant because they not only have excellent piezoelectric properties, but also maintain a high Curie temperature. Similar to PZT piezoceramics, the optimal piezoelectric properties of BS-PT solid solution are obtained

in the morphotropic phase boundary (MPB) region, with a high piezoelectric coefficient d_{33} = 460 pC/N, which is similar to that of traditional PZT-based piezoelectric ceramics, but the Curie temperature T_c is as high as 450 °C [8–10]. In order to further improve on these piezoelectric properties, numerous modifications have been reported. The research on these modifications can mainly be divided into covering three methods: one is single-element doping, the second is composite-ion doping, and the third involves the introduction of a third solid-solution system. Since single-element doping and composite-ion doping struggle to achieve accurate adjustment of performance, the introduction of a third component has become a current research hot spot. Lead-based relaxor ferroelectrics, the general formula of which is $Pb(B_1,B_2)O_3$, where B_1 represents low-valence cations (such as Mg, Zn, Fe, Ni, Yb, Cd, etc.) and B_2 represents high-valence cations (such as Nb, Sb, Ta, etc.), are usually selected as a third component to be introduced into a BS-PT system due to their excellent dielectric and piezoelectric properties [11–13]. The introduction of relaxor ferroelectric end members not only improves the relaxor characteristics and electrical properties, but also can form a ternary solid solution formed with the BS-PT system, and extend its MPB region from a point to a line, which can achieve performance regulation in a wider range. In 2002, Ryu Jungho et al. studied the ternary system of $BiScO_3$-$PbTiO_3$-$Pb(Mn_{1/3}Nb_{2/3})O_3$ by means of solid-phase synthesis [14]. The results show that in the ternary system of $(0.9-x)$ $BiScO_3$-$xPbTiO_3$-0.1$Pb(Mn_{1/3}Nb_{2/3})O_3$, the MPB shifts to x = 0.6, which is slightly lower than the value of 0.64 for BS-PT. The piezoelectric constant and electromechanical coupling coefficient near MPB are 220pC/N and 0.34, respectively. The mechanical quality factor of the system is significantly improved, reaching 1000 at x = 0.68, and the Curie temperature at this point also reaches 420 °C. In 2008, the study of a $Pb(Sc_{1/2}Nb_{1/2})O_3$-$BiScO_3$-$PbTiO_3$ ternary system was reported [15]. The main performance parameters of the $Pb(Sc_{1/2}Nb_{1/2})O_3$ ternary system were d_{33} = 453pC/N, k_p = 0.58, and T_c = 405 °C. However, its thermal stability is poor. In general, high-voltage electrical activity and good thermal stability do not easily coexist, which affects the practical application of materials [16]. This experiment hopes that through the application of the solid solution of the third component, under the premise of high piezoelectric activity, the material will have good thermal stability, so that it can better meet the requirements for practical applications. In this experiment, the third component was selected by considering the tolerance factor.

The tolerance factor is the most important parameter used to characterize the structural stability and Curie temperature of materials [17]. In general, the perovskite structure with a low tolerance factor usually has a high Curie temperature, and when the tolerance factor is closer to 1, the component is more easily dissolved as the third component. $Pb(Yb_{1/2}Nb_{1/2})O_3$, which has a low tolerance factor of 0.951, forms a solid solution with PT material with a Curie temperature of 360 °C in the MPB region. Therefore, in this work, a $Pb(Yb_{1/2}Nb_{1/2})O_3$ end member was selected as the third component to form a ternary solid solution with BS-PT ceramics, in order to improve its piezoelectric properties while reducing the Curie temperature slightly, and meet the requirements for the application of high-performance piezoelectric ceramics in high-temperature environments [18].

2. Experimental Procedures

The $0.025Pb(Yb_{1/2}Nb_{1/2})O_3$-$(0.975-x)BiScO_3$-$xPbTiO_3$ (PYN-BS-xPT) ternary piezoelectric ceramics were synthesized via the traditional solid-state reaction method. High-purity raw materials of Bi_2O_3 (99.9%,), Sc_2O_3 (99.9%), PbO (99.9%), TiO_2 (99%), Yb_2O_3 (99.9%), and Nb_2O_3 (99.99%) were weighed according to the stoichiometric ratio [16]. The raw materials used in this experiment were obtained from Shanghai Aladdin Biotechnology Co., Ltd.(Shanghai, China). For the purpose of preventing the generation of a pyrochlore phase, the precursor of $Yb_2Nb_2O_8$ was prepared by means of the reaction of Yb_2O_3 and Nb_2O_5 before the reaction with PbO. To compensate for the evaporation of Pb and Bi ions during high-temperature sintering, an excess of 1 wt% of Bi_2O_3 and PbO each was added to ensure that the desired composition was obtained [19]. The weighed powders were

ball-milled with ethanol for 16 h, and then the slurry was dried in an oven at a temperature of 80 °C [20]. Subsequently, the powder was placed in crucibles and heated up to 850 °C at a speed of 4 °C/min for 4 h. The calcined powder was ball milled again using the same procedure, and a polyvinyl alcohol (PVA) binder was added and scalped using a 100-mesh sizer. The powder was compressed at a pressure of 150 Mpa to form samples with a diameter of 12 mm and a thickness of 1 mm [21,22]. The samples were heated up to 600 °C at a speed of 1 °C/min to remove the PVA binder. Subsequently, the samples were placed on Al_2O_3 plates and evenly covered with powder of the same composition. The samples were heated up to 1100 °C–1150 °C at a speed of 2 °C/min and held for 3 h for sintering, and finally cooled naturally to room temperature. After polishing, a uniform layer of silver paste was coated on the surface of the sintered samples and heated up to 580 °C for 10 min [23,24].

After polishing, the density of the ceramic samples obtained at different sintering temperatures was measured according to the Archimedes drainage method. The formula is as follows:

$$\rho = \frac{m_1}{m_3 - m_2} \times \rho_w \quad (1)$$

In this formula, m_1 is the weight of the dried ceramic sample, m_2 is the weight of the ceramic sample in deionized water, and m_3 is the weight of the ceramic sample after wiping off the surface moisture.

After the density test of the ceramic sample, the sintering temperature with the highest density was selected as the optimal sintering temperature for subsequent experiments.

The phase analysis of the sample was carried out using the PANalytiacal X'Pert PW3050/60 X-ray diffractometer produced by Philips in the Netherlands. The microstructural morphology of the sample was observed and analyzed via field-emission scanning electron microscopy (Quanta450FEG, FEI Company, Hillsboro, OR, USA) [25]. After the ceramic samples were polarized in silicone oil at 120 °C for 30 min, the piezoelectric coefficient of the samples was measured using a quasi-static d_{33} measuring instrument produced by the Institute of Acoustics, Chinese Academy of Sciences (Beijing, China) [26]. The resonance-antiresonance frequency of the sample was measured using an HP4294A precision impedance analyzer (Agilent Technologies, Inc., Santa Clara, CA, USA). The dielectric temperature spectrum of the sample was tested using the impedance analyzer produced by Agilent company and the intelligent temperature controller system (Santa Clara, CA, USA). The ferroelectric hysteresis (*P*–*E*) loops was measured using an exactitude workstation produced by Polyk in the United States (State College, PA, USA) [27]. In addition, the stability of the sample was characterized in this experiment, including cycle stability and temperature stability test.

3. Results and Discussion

3.1. Structure and Phase Analysis

The bulk density of ceramics can reflect the density of ceramic samples after sintering, and can reflect the compactness and porosity of the internal grain arrangement of ceramic samples to a certain extent. Figure 1 shows the density of ceramic samples at different sintering temperatures. It can be seen from the diagram that the density of the ceramic sample increases first and then decreases with the increase in the sintering temperature under the same component, and the maximum value is obtained at 1130 °C. Therefore, we choose 1130 °C as the best sintering temperature for PYN-BS-PT ceramics.

Figure 2a presents the XRD pattern of PYN-(0.975−*x*)BS-*x*PT (PYN-BS-*x*PT) piezoelectric ceramics, and Figure 2b presents the {200} peak amplification diagram of PYN-BS-*x*PT ceramics, where R represents the rhombohedral phase and T represents the tetragonal phase. It can be observed that all the samples show a perovskite structure without the presence of a second phase, indicating that the third component PYN has completely entered the BS-PT system and formed a steady solid solution. With the increase in PT content, the lattice symmetry of PYN-BS-*x*PT piezoelectric ceramics gradually changed. When x = 0.60,

the (200) diffraction peak of the PYN-BS-xPT ceramic is a single diffraction peak, indicating that the x = 0.60 ceramic has an R phase. With the increase in PT content, the (200) peak gradually widens and splits, and completely splits into two diffraction peaks (002)/(200) in the x = 0.62 ceramic, indicating that the phase structure of the PYN-BS-xPT ceramic shifted from an R phase to a T phase [28]. As shown in Figure 2b, when $x < 0.61$, the material is a rhombohedral phase; when $x > 0.61$, the material is a tetragonal phase. When x = 0.61, the material is in a two-phase coexistence state—that is, there is a morphotropic phase boundary region, which is beneficial for obtaining high dielectric and piezoelectric properties. This is different from the MPB region of the pure (1−x)BS-xPT system located at x = 0.64, due to the introduction of $Yb^{3+}$and Nb^{5+} cations in the PYN system which replace the $Sc^{3+}$and Ti^{4+} ions, resulting in a slight shift in the MPB region [29].

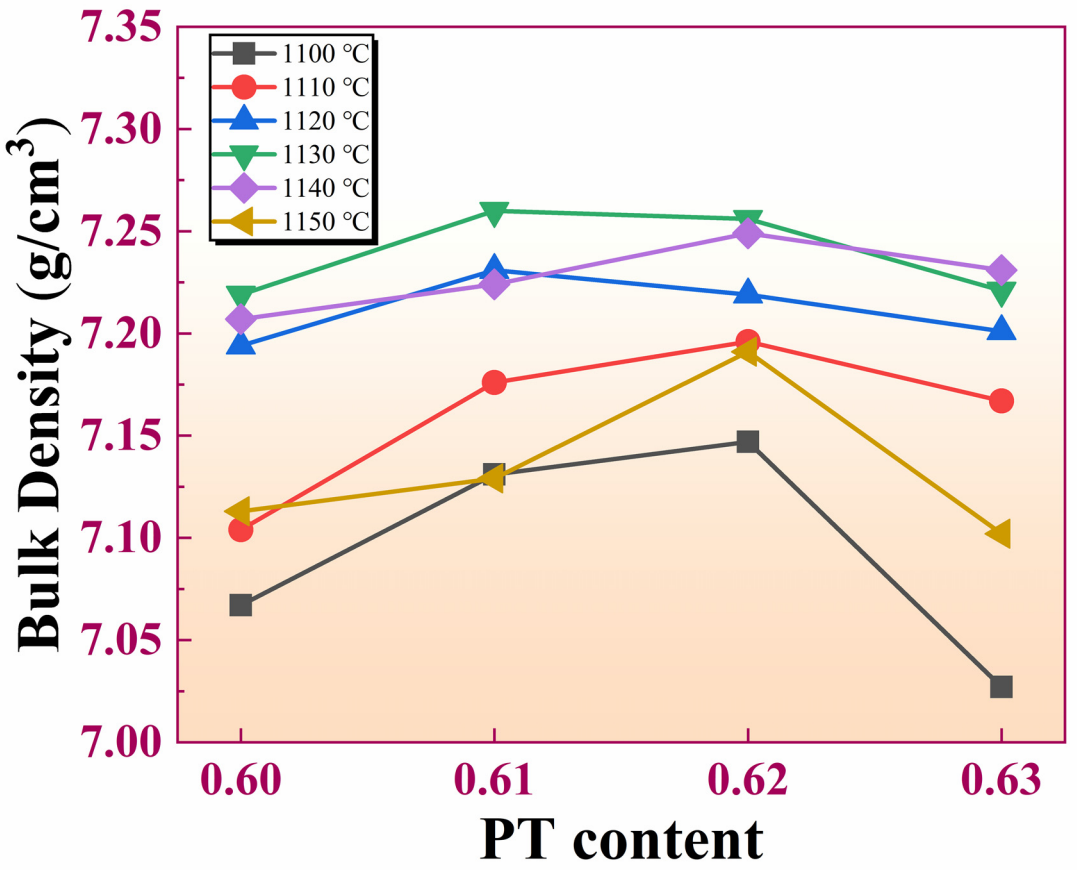

Figure 1. Density of ceramic samples sintered at different temperatures.

Figure 3 is the SEM image of the PYN-BS-xPT peizoelectric ceramics. It can be observed that the microstructure of all of the samples is uniform, dense, and has no obvious pores, indicating that the sintering temperature is suitable. The dense and uniform ceramic material is the basis for its excellent piezoelectric and mechanical properties [30]. The grain size of PYN-BS-xPT ceramics was statistically analyzed and the results are shown in the inset. There is no significant change in grain size as the PT content increases from x = 0.60 to x = 0.63, with an average grain size of 2.69 μm and 3.01 μm, respectively.

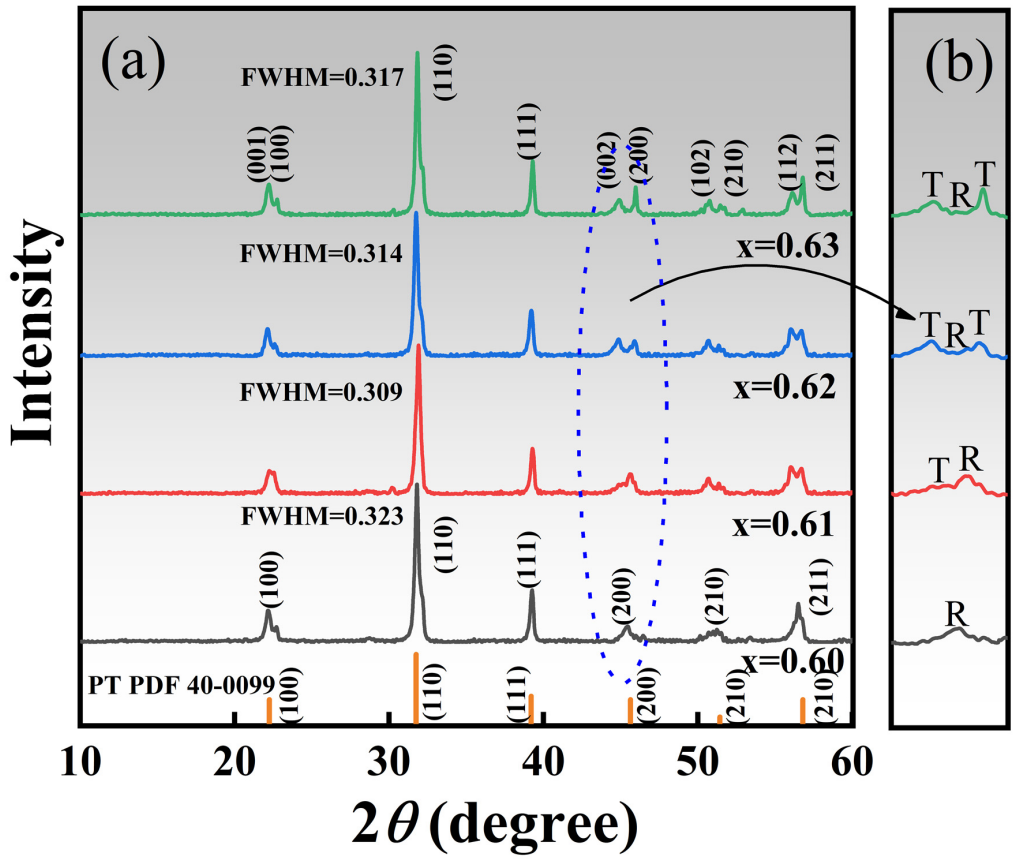

Figure 2. (**a**) XRD patterns and (**b**) magnified {200} peak of the PYN-BS-*x*PT ceramics.

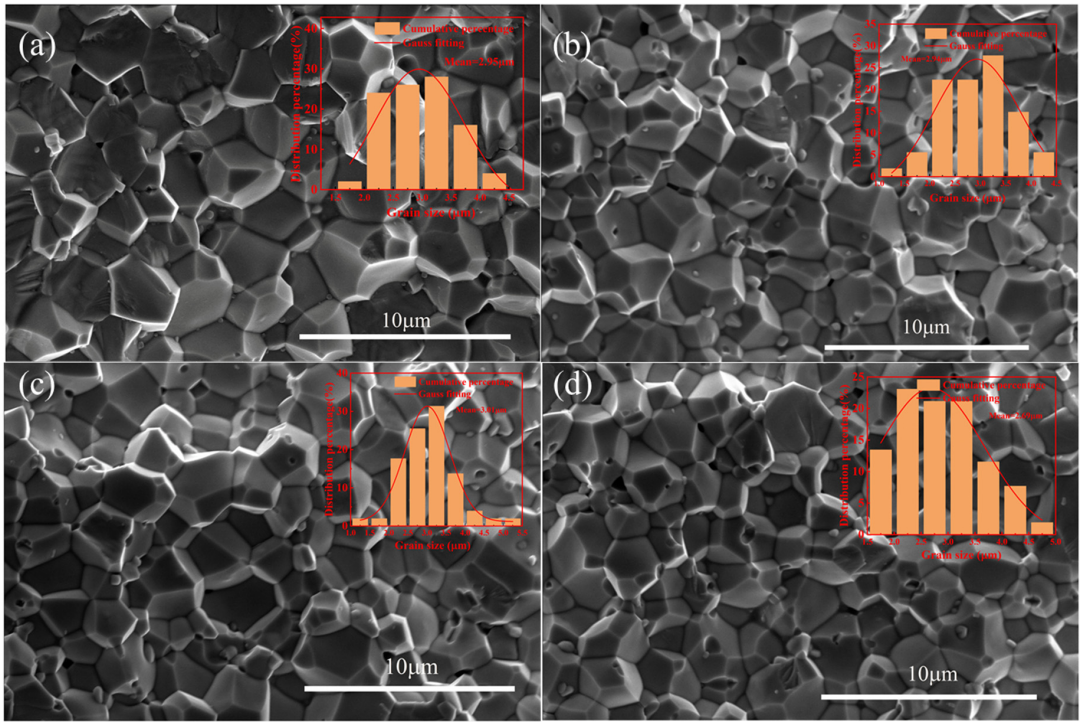

Figure 3. SEM micrographs of the PYN-BS-*x*PT ceramics: (**a**) x = 0.60; (**b**) x = 0.61; (**c**) x = 0.62; (**d**) x = 0.63. The insets show the grain size distribution of the ceramics.

3.2. Dielectric Behavior

Figure 4 shows the dielectric constant and dielectric loss of PYN-BS-*x*PT ceramics at different temperature and frequencies. It can be seen that the dielectric constant has a dielectric anomaly at the ferroelectric to paraelectric phase transition point—that is, the Curie temperature [31]. The Curie temperature of PYN-BS-*x*PT ceramics increases linearly with the increase in PT content, from 412 °C for x = 0.60 to 424 °C for x = 0.63, which is slightly lower than that of the BS-PT solid solution, indicating that the introduction of PYN will decrease the Curie temperature of BS-PT ceramics [32]. At the same time, the dielectric temperature spectrum of PYN-BS-*x*PT ceramics shows a significant broadening peak, and the degree of broadening with the increase in PT content gradually decreases. As a typical relaxor ferroelectric end member, PYN is introduced into the BS-PT binary system to enhance its relaxor properties, which can be demonstrated by the dielectric temperature spectrum at different frequencies, as shown in Figure 4b. The dielectric constant of PYN-BS-0.61PT ceramics shows a relatively wide peak and the Curie temperature gradually moves in the high-frequency direction. All of the results show that the incorporation of PYN provides the ternary PYN-BS-0.61PT ceramics with relaxor characteristics, as a typical perovskite-type relaxor ferroelectric. This result is mainly due to the unequal substitution of Yb^{3+} and Nb^{5+} ions, which destroys the balance of the internal valence, may lead to chemical heterogeneity and structural disorder, and finally causes the relaxation behavior of PYN-BS-0.61PT. The dielectric loss shows the same trend as the dielectric temperature. When x = 0.61, the dielectric loss at room temperature decreases from 0.05 to only 0.0149. Compared with the doped BS-PT binary piezoelectric ceramics, the dielectric loss is greatly improved [33]. This shows that the doped ternary system piezoelectric ceramics can better meet the application requirements.

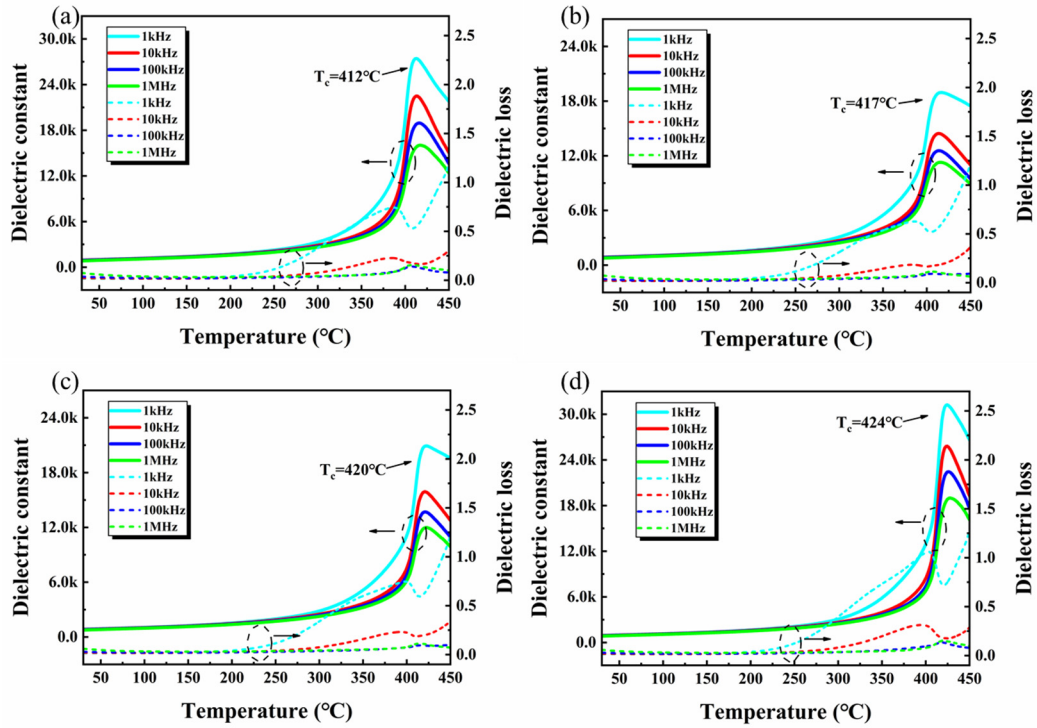

Figure 4. Temperature dependence of the dielectric response of the PYN-BS-*x*PT ceramics: (**a**) x = 0.60; (**b**) x = 0.61; (**c**) x = 0.62; (**d**) x = 0.63.

3.3. Piezoelectric and Ferroelectric Properties

Figure 5 shows the piezoelectric coefficient d_{33} and planar electromechanical coupling factor k_p of PYN-BS-xPT piezoelectric ceramics, and the k_p is calculated based on the following formula:

$$\frac{1}{k_p^2} = 0.398\frac{f_r}{f_a - f_r} + 0.579 \quad (2)$$

where f_a is the antiresonance frequency and f_r is the resonance frequency [34]. It can be observed that the piezoelectric d_{33} and k_p of PYN-BS-xPT ceramics show the same trend—that is, increasing first and then decreasing with an increase in PT composition. The best piezoelectric properties were observed at $x = 0.61$ with $d_{33} = 370$ pC/N and $k_p = 0.44$. This is consistent with the results of XRD patterns, further proving that the optimal piezoelectric properties are obtained at $x = 0.61$ in the MPB region, where the R phase and T phase coexist, and the polarization intensity shows more equivalent energy states. The R phase has eight equivalent energy states on the [111] polar axis, and T phase has six equivalent energy states on the [100] polar axis. For the MPB region where two phases coexist, 14 equivalent energy states can be converted into each other under a low energy level, which is beneficial for improving the polarization and piezoelectric properties [35,36].

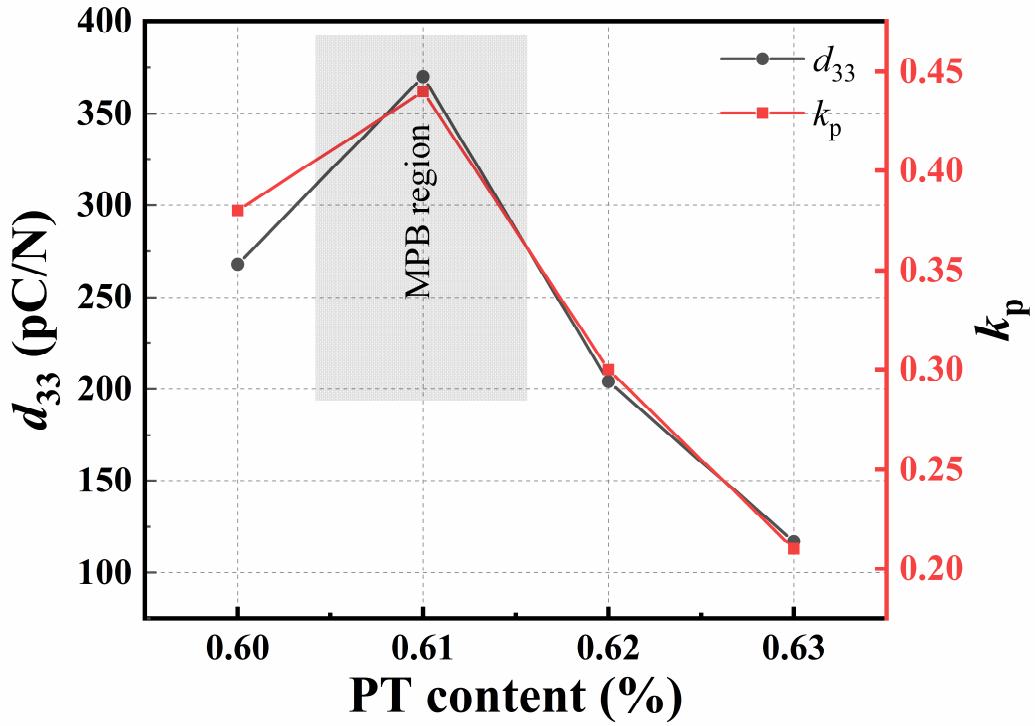

Figure 5. Piezoelectric coefficient d_{33} and planar electromechanical coupling factor k_p for PYN-BS-xPT ceramics.

Figure 6a displays the P–E loops of PYN-BS-xPT peizoelectric ceramics. It can be observed that all samples show a saturated P–E loop without obvious leakage behavior. The remanent polarization P_r and coercive field E_c are extracted as shown in Figure 6b. The P_r increases with the increase in PT content, reaching a maximum value of 33.9 μC/cm^2 at $x = 0.61$, and then gradually decreases to 20.8 μC/cm^2 at $x = 0.63$. The highest value obtained for the $x = 0.61$ ceramic further proves that it is located in the MPB region. Compared with the unmodified BS-PT binary system, P_r is greatly improved, which proves that the introduction of PYN optimizes the ferroelectric properties of BS-PT.

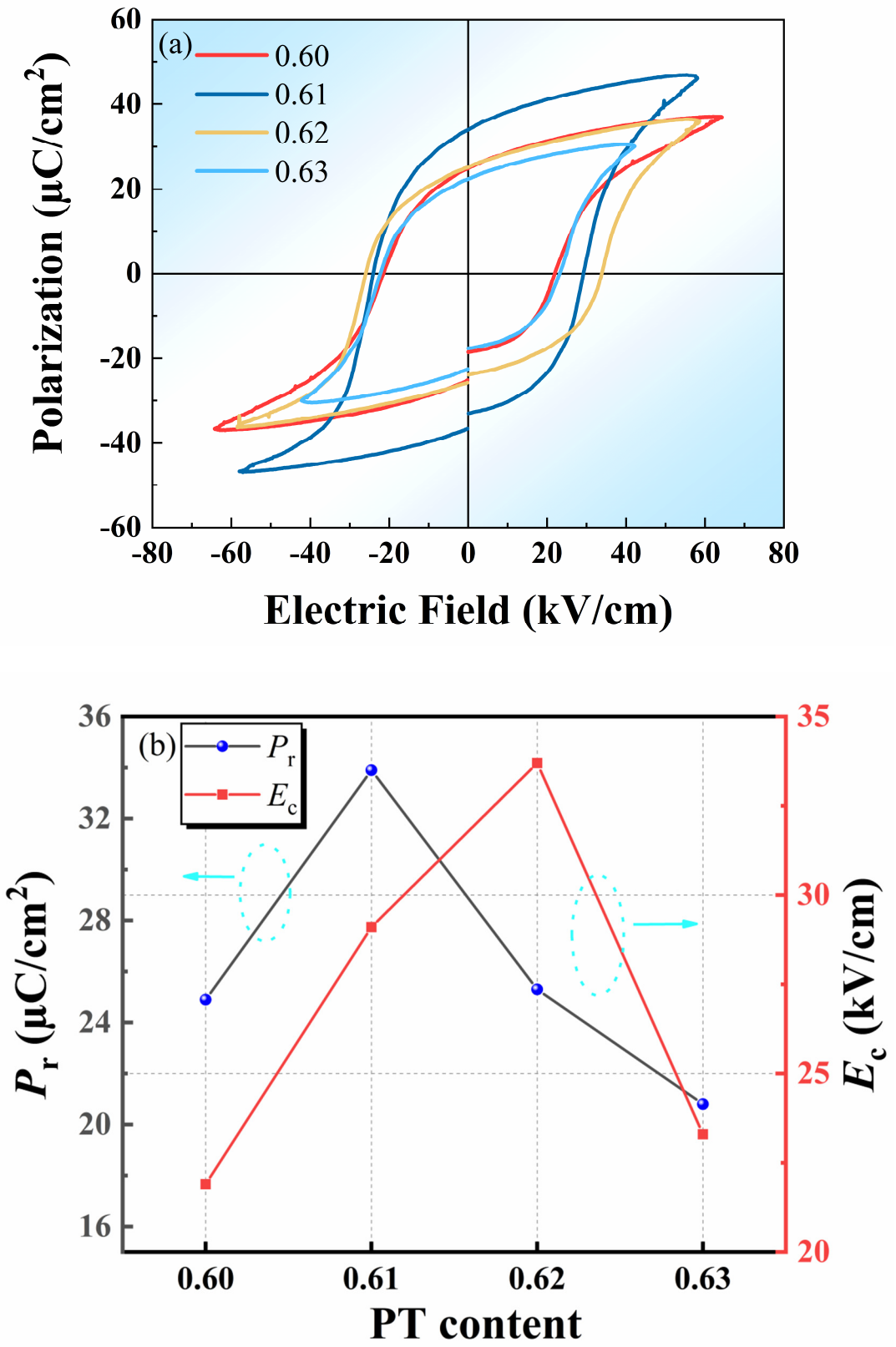

Figure 6. (**a**) Polarization hysteresis loops of the PYN-BS-*x*PT ceramics, (**b**) remanent polarization P_r and coercive field E_c of the PYN-BS-*x*PT ceramics.

The electric field-induced strain of the piezoelectric material is an important parameter in the design of the actuator, which comes from the intrinsic contribution provided by the inverse piezoelectric effect and the extrinsic contribution caused by the domain wall

motion [37]. Figure 7 presents the electric field-induced strain curve of the PYN-BS-*x*PT ceramic. The larger the electro-induced strain is, the larger the driving displacement under the same voltage is. In this experiment, all ceramic samples maintained good linearity and achieved a maximum strain of 0.17% at room temperature, indicating that the component is very suitable for the design of high-temperature piezoelectric actuators.

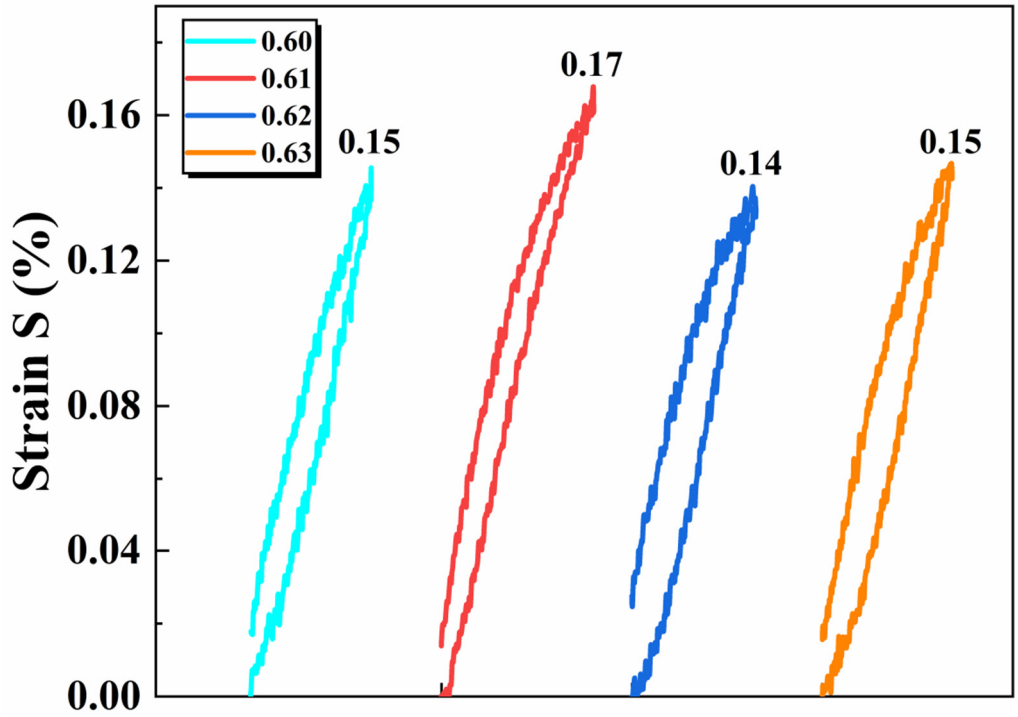

Figure 7. The electric field-induced strain curve of PYN-BS-*x*PT.

3.4. Stability Analysis

The cyclic stability of ceramics is one of the key parameters for their service life and reliability [38,39]. Figure 8 shows the *P–E* cycling stability of PYN-BS-0.61PT at room temperature. It can be observed that after 10^5 cycles, the *P–E* curve of the ceramic is still in a saturated state, and there is no obvious leakage phenomenon. There is no significant change in the *P–E* curve compared with the *P–E* curve before the cycle, which indicates that the PYN-BS-*x*PT ceramics have excellent stability and reliability in long-term use.

To further explore the temperature stability of piezoelectric properties, the piezoelectric d_{33} of PYN-BS-*x*PT ceramics at different annealing temperatures was characterized, as shown in Figure 9. All PYN-BS-*x*PT ceramic samples exhibited a stable d_{33} with the increase in annealing temperature, and this decreased sharply after reaching the depolarization temperature. It is worth noting that the PYN-BS-0.61PT ceramic with a high piezoelectric d_{33} = 370 pC/N displayed no significant attenuation in the range of room temperature to 290 °C, showing its potential for application in piezoelectric devices with variable temperature [40].

In order to further study the strain–temperature stability of PYN-BS-*x*PT ceramics, we measured the field-induced strain of ceramic samples with x = 0.61 in the temperature range of 30 °C–240 °C. The measurement results are shown in Figure 10. It can be seen from the diagram that the change rate of field-induced strain of the ceramic sample with temperature is about 3%, showing good temperature stability. In summary, the temperature stability of PYN-BS-*x*PT is much higher than that of commercial ceramics such as PZT 5H, PZT 4 and PNN-PZ-PT, and it is an ideal material for application in the field of wide-temperature-range and high-performance piezoelectric actuators.

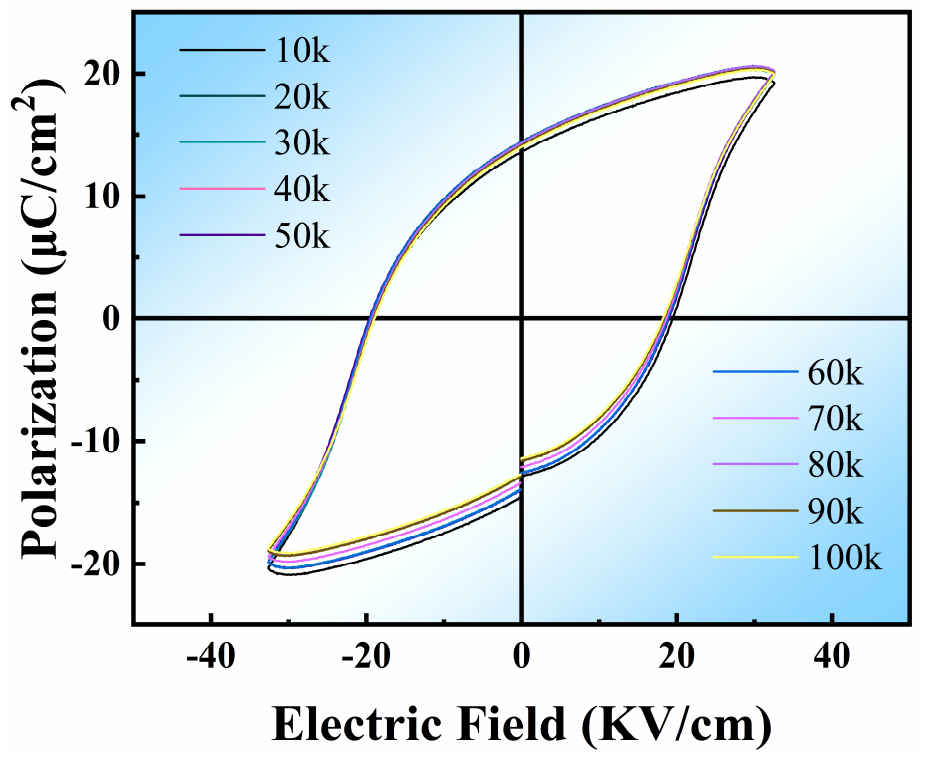

Figure 8. P–E cycle stability of PYN-BS-0.61PT at room temperature.

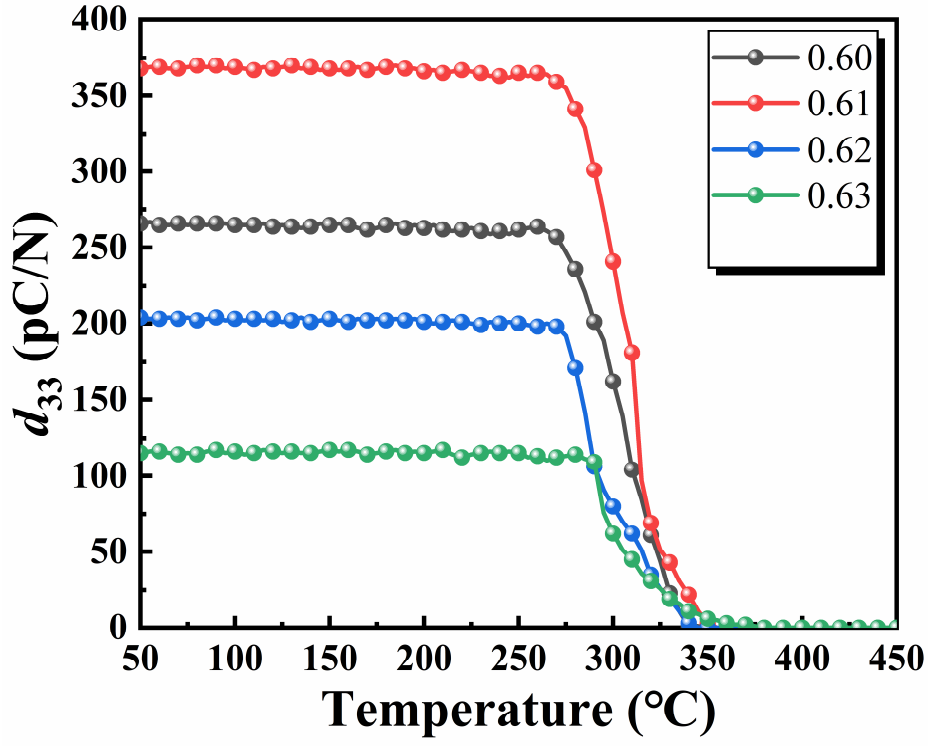

Figure 9. Temperature stability of the piezoelectric coefficient for PYN-BS-*x*PT ceramics.

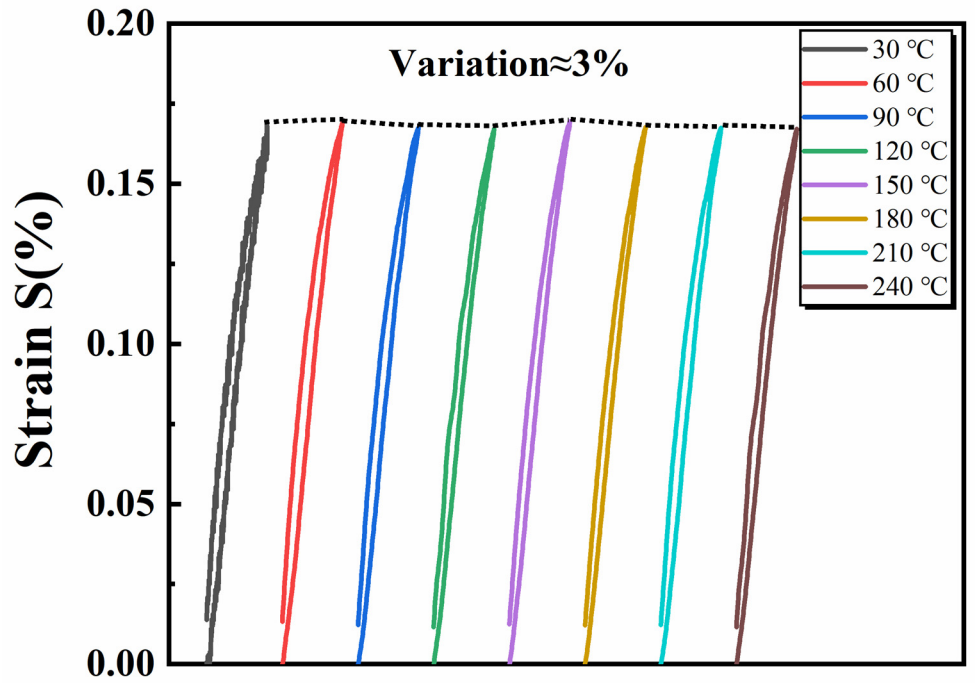

Figure 10. The variation trend of the electric field-induced strain curve of PYN-BS-61PT with temperature.

4. Conclusions

In summary, PYN-BS-xPT ($0.60 \leq x \leq 0.63$) ternary system ceramics were prepared by means of the solid-state sintering method. The effects of PYN and PT contents on the phase structure, microstructure, dielectric, ferroelectric and piezoelectric properties of PYN-BS-xPT ceramics were systematically studied. The XRD and SEM results show that a PYN end member can be completely integrated into the BS-PT system and form a dense and uniform microstructure. The best piezoelectric properties are obtained in the MPB region $x = 0.61$ where rhombohedral and tetragonal phases coexist, with the d_{33}, k_p and ε_r being 370 pC/N, 0.44 and 878, respectively. Good fatigue resistance is observed in the unipolar stain fatigue curve, accompanied by a low reduction from 1 to more than 10^5 cycles. Outstanding temperature stability from room temperature to 290 °C is observed for the $x = 0.61$ ceramic, due to its high Curie temperature $T_c = 417$ °C. In traditional piezoelectric ceramics, although the morphotropic phase boundary region has high piezoelectric activity, it generally has poor thermal stability. The ceramic produced in this work not only have high piezoelectric activity, but also exhibit good thermal stability, which is one of the highlights of this experiment. In addition, this experiment uses the traditional solid-phase sintering method, which is simple, low-cost, and helpful for large-scale industrial production in the future. All of the results show that PYN-modified BS-PT ceramics have excellent piezoelectric activity and thermal stability, making them ideal piezoelectric materials suitable for application in high-temperature environments.

Author Contributions: Data curation, F.Z. and H.H.; project administration, H.H. and H.L.; supervision, H.H. and H.L.; writing—original draft, F.Z. and H.H.; writing—review and editing, F.Z., H.H., M.C., Z.Y., S.F. and H.L. All authors have read and agreed to the published version of the manuscript.

Funding: This work was funded by the National Key Research and Development Program of China (No. 2023YFB3812200) and Guangdong Basic and Applied Basic Research Foundation (2021A1515110060, 2022A1515010073 and 2022B1515120041), Major Program of the Natural Science Foundation of China (51790490).

Data Availability Statement: All data generated or analyzed during this study are contained in this article.

Conflicts of Interest: The authors declare no conflicts of interest.

References

1. Zhao, H.; Yu, X.; Li, F.; Yang, H.; Guo, Q.; Zhang, Z. Large Piezoelectricity with Enhanced Thermal Stability in $BiScO_3$-$BiInO_3$-$PbTiO_3$ Ternary Perovskite Ceramics. *Ceram. Int.* **2023**, *49*, 40953–40959. [CrossRef]
2. Dai, Z.; Liu, W.; Lin, D.; Ren, X. Electrical Properties of Zirconium-Modified $BiScO_3$-$PbTiO_3$ Piezoelectric Ceramics at Re-Designed Phase Boundary. *Mater. Lett.* **2018**, *215*, 46–49. [CrossRef]
3. Kang, W.; Li, Y.; Zheng, Z.; Zhao, R. Enhanced Dielectric and Piezoelectric Performance of $(1-x)Bi_{0.5}(Na_{0.78}K_{0.22})_{0.5}TiO_3$-$xBaTiO_3$ Ceramics. *Ceram. Int.* **2020**, *46*, 18089–18095. [CrossRef]
4. Feng, Y.; Yang, C.; Guo, X.; Sun, W.; Wang, W.; Lin, X.; Huang, S. Achieving Both Large Piezoelectric Constant and Low Dielectric Loss in $BiScO_3$-$PbTiO_3$–$Bi(Mn_{2/3}Sb_{1/3})O_3$ High-Temperature Piezoelectric Ceramics. *J. Adv. Dielectr.* **2022**, *12*, 2250017. [CrossRef]
5. Zhao, T.; Shi, K.; Fei, C.; Sun, X.; Quan, Y.; Liu, W.; Zhang, J.; Dai, X. Structure, Electrical Properties, and Thermal Stability of the Mn/Nb Co-Doped Aurivillius-Type $Na_{0.5}Bi_{4.5}Ti_4O_{15}$ High Temperature Piezoelectric Ceramics. *Crystals* **2023**, *13*, 433. [CrossRef]
6. Mitsui, R.; Fujii, I.; Nakashima, K.; Kumada, N.; Kuroiwa, Y.; Wada, S. Chemical Composition Dependence of Ferroelectric Properties for $BaTiO_3$-$Bi(Mg_{1/2}Ti_{1/2})O_3$-$BiFeO_3$ Lead-Free Piezoelectric Ceramics. *J. Ceram. Soc. Jpn.* **2013**, *121*, 855–858. [CrossRef]
7. Liao, W.; Lu, Y.; He, X.; Li, T.; Liang, L.; Liu, X.; Li, H.; Liu, Y.; Zhou, L. High Piezoelectricity of Multicomponent Lead-Based Ceramics with High Temperature Stability. *ACS Appl. Electron. Mater.* **2023**, *5*, 6124–6133. [CrossRef]
8. Dong, Y.; Zou, K.; Liang, R.; Zhou, Z. Review of $BiScO_3$-$PbTiO_3$ Piezoelectric Materials for High Temperature Applications: Fundamental, Progress, and Perspective. *Prog. Mater. Sci.* **2023**, *132*, 101026. [CrossRef]
9. Hu, Q.; Wang, Y.; Wu, L.; Yin, J.; Chen, L.; Yuan, G.; Yang, Y. Effects of $LiNbO_3$ Doping on the Microstructures and Electrical Properties of $BiScO_3$–$PbTiO_3$ Piezoelectric System. *J. Mater. Sci. Mater. Electron.* **2018**, *29*, 18036–18044. [CrossRef]
10. Zhang, L.; Li, S.; Zhu, Z.; Rui, G.; Du, B.; Chen, D.; Huang, Y.F.; Zhu, L. Recent Progress on Structure Manipulation of Poly(Vinylidene Fluoride)-Based Ferroelectric Polymers for Enhanced Piezoelectricity and Applications. *Adv. Funct. Mater.* **2023**, *33*, 2301302. [CrossRef]
11. Gao, M.; Yu, Z.; Fu, J.; Zhang, Y.; Zuo, R. Enhanced Piezoelectricity and Excellent Thermal Stability in Modified $BiFeO_3$–$PbTiO_3$-Based High-Temperature Piezoelectric Ceramics. *J. Mater. Sci. Mater. Electron.* **2023**, *34*, 1085. [CrossRef]
12. Kumar, A.; Hussain, A.; Joseph, A.J.; Goel, S.; Gupta, R.; Singh, N.S.; Singh, U. Synthesis of Ternary 0.49BF-0.20PMN-0.31PT Ceramic at Morphotropic Phase Boundary for Excellent Die-/Piezo-/Ferro-/Pyro-Electric Response. *Appl. Phys. A Mater. Sci. Process* **2022**, *128*, 655. [CrossRef]
13. Zheng, F.; Tian, X.; Fang, Z.; Lin, J.; Lu, Y.; Gao, W.; Xin, R.; Fu, D.; Qi, Y.; Ma, Z.; et al. Sm-Doped PIN-PMN-PT Transparent Ceramics with High Curie Temperature, Good Piezoelectricity, and Excellent Electro-Optical Properties. *ACS Appl. Mater. Interfaces* **2023**, *15*, 7053–7062. [CrossRef] [PubMed]
14. Ryu, J.; Priya, S.; Sakaki, C.; Uchino, K. High Power Piezoelectric Characteristics of $BiScO_3$-$PbTiO_3$-$Pb(Mn_{1/3}Nb_{2/3})O_3$. *Jpn. J. Appl. Phys.* **2002**, *41*, 6040–6044. [CrossRef]
15. Yao, Z.; Liu, H.; Liu, Y.; Li, Z.; Cheng, X.; Cao, M.; Hao, H. Morphotropic Phase Boundary in $Pb(Sc_{1/2}Nb_{1/2})O_3$-$BiScO_3$-$PbTiO_3$ High Temperature Piezoelectrics. *Mater. Lett.* **2008**, *62*, 4449–4451. [CrossRef]
16. Liu, G.; Kong, L.; Hu, Q.; Zhang, S. Diffused Morphotropic Phase Boundary in Relaxor-$PbTiO_3$crystals: High Piezoelectricity with Improved Thermal Stability. *Appl. Phys. Rev.* **2020**, *7*, 021405. [CrossRef]
17. Han, X.; Wei, L.; Yang, Z.; Zhang, T. Phase Formation, Dielectric and Ferroelectric Properties of $Ca_xBa_{1-x}Nb_2O_6$ Ceramics. *Ceram. Int.* **2013**, *39*, 4853–4860. [CrossRef]
18. Lan, Z.; Chen, K.; He, X.; Zhou, S.; Zheng, X.; Liu, J.; Fang, L.; Lei, X.; Wang, D.; Peng, B.; et al. Phase Evolution and Thermal Stability of High Curie Temperature $BiScO_3$-$PbTiO_3$-$Pb(Cd_{1/3}Nb_{2/3})O_3$ Ceramics near MPB. *J. Appl. Phys.* **2019**, *126*, 234103. [CrossRef]
19. Ginting, F.H.S.; Tetuko, A.P.; Asri, N.S.; Nurdiyansah, L.F.; Setiadi, E.A.; Humaidi, S.; Sebayang, P. Surface Treatment on Metal Foam Wick of a Ferrofluid Heat Pipe. *Surf. Interfaces* **2023**, *36*, 102499. [CrossRef]
20. Ren, X.; Liu, X.; Tang, M.; Wang, Y.; Xu, Z.; Yan, Y. Enhanced Electromechanical Properties and Thermal Stability of Antimony-Modified $BiScO_3$-$PbTiO_3$ High-Temperature Piezoelectric Ceramics. *Ceram. Int.* **2023**, *49*, 25658–25664. [CrossRef]
21. Liu, R.; Chu, X.; Su, J.; Fu, X.; Kan, Q.; Wang, X.; Zhang, X. Enzyme-Assisted Ultrasonic Extraction of Total Flavonoids from *Acanthopanax senticosus* and Their Enrichment and Antioxidant Properties. *Processes* **2021**, *9*, 1708. [CrossRef]
22. Son, S.; Lee, J.; Asghari-Rad, P.; Kim, R.E.; Park, H.; Jang, J.I.; Chen, W.; Heo, Y.U.; Kim, H.S. Hierarchically Heterogeneous Microstructure and Mechanical Behavior of the Multi-Materials Prepared by Powder Severe Plastic Deformation. *Mater. Res. Lett.* **2023**, *11*, 915–924. [CrossRef]
23. Li, C.X.; Hong, Y.N.; Yang, B.; Zhang, S.T.; Liu, D.Q.; Wang, X.M.; Liu, Q.; Zhao, L.; Cao, W.W. Phase Transition, Ferroelectric and Piezoelectric Properties of B-Site Complex Cations $(Fe_{0.5}Nb_{0.5})^{4+}$-Modified $Ba_{0.70}Ca_{0.30}TiO_3$ Ceramics. *Ceram. Int.* **2020**, *46*, 9519–9529. [CrossRef]
24. Liu, H.; Hu, J.; Zhang, Y.; Zhao, J.; Wang, X.; Song, J. A Dual Role of D-Sorbitol in Crystallizing and Processing Poly (Lactic Acid). *J. Polym. Res.* **2023**, *30*, 102. [CrossRef]
25. Phelan, D.; Long, X.; Xie, Y.; Ye, Z.G.; Glazer, A.M.; Yokota, H.; Thomas, P.A.; Gehring, P.M. Single Crystal Study of Competing Rhombohedral and Monoclinic Order in Lead Zirconate Titanate. *Phys. Rev. Lett.* **2010**, *105*, 207601. [CrossRef]

26. Yue, Y.; Zhang, Q.; Nie, R.; Yu, P.; Chen, Q.; Liu, H.; Zhu, J.; Xiao, D.; Song, H. Influence of Sintering Temperature on Phase Structure and Electrical Properties of 0.55Pb($Ni_{1/3}Nb_{2/3}$)O_3–0.45Pb($Zr_{0.3}Ti_{0.7}$)O_3 Ceramics. *Mater. Res. Bull.* **2017**, *92*, 123–128. [CrossRef]
27. Cheng, H.; Zhou, W.; Du, H.; Luo, F.; Zhu, D.; Jiang, D.; Xu, B. Enhanced Dielectric Relaxor Properties in (1 − x)($K_{0.5}Na_{0.5}$)NbO_3-x($Ba_{0.6}Sr_{0.4}$)$_{0.7}Bi_{0.2}TiO_3$ Lead-Free Ceramic. *J. Alloy. Compd.* **2013**, *579*, 192–197. [CrossRef]
28. Talanov, M.V.; Bush, A.A.; Kamentsev, K.E.; Sirotinkin, V.P.; Segalla, A.G. Structure, Dielectric and Piezoelectric Properties of the $BiScO_3$-$PbTiO_3$-$PbMg_{1/3}Nb_{2/3}O_3$ Ceramics. *Ferroelectrics* **2019**, *538*, 105–112. [CrossRef]
29. Chen, Y.; Shi, H.; Zhang, M.; Zhang, D.; Li, Z.; Xu, Y.; Jin, L.; Yan, Y. Comprehensive Properties and Thermal Stability of Ta_2O_5-Doped PIN-PHT Ceramics. *Ceram. Int.* **2022**, *48*, 32908–32916. [CrossRef]
30. Gezimu, G.; Taddesse, P.; Chufamo, A.; Lewetegn, K.; Tilahun, B.; Zinabe, B.; Babu, K.V.; Saxena, S. Nanostructured $Ni_{0.8}Co_{0.2}Mn_xFe_{2-x}O_4$ Ferrites: Structural, Elastic, Optical, and Electromagnetic Properties. *J. Indian Chem. Soc.* **2023**, *100*, 101103. [CrossRef]
31. Qaiser, M.A.; Ma, X.Z.; Ma, R.; Ali, W.; Xu, X.; Yuan, G.; Chen, L. High-Temperature Multilayer Actuators Based on CuO Added $BiScO_3$–$PbTiO_3$ Piezoceramics and Ag Electrodes. *J. Am. Ceram. Soc.* **2019**, *102*, 5424–5431. [CrossRef]
32. Ma, P.; Zhang, Z.; Liu, X.; Shi, X.; Prashanth, K.; Jia, Y. Microstructure and Nanoindentation Creep Behavior of Binary Al-Cu Alloy Synthesized at High Pressure. *JOM* **2023**, *75*, 176–183. [CrossRef]
33. Li, Z.-W.; Ma, M.-G.; Li, C.-B.; Chen, Z.-H.; Xu, J.-J. Effect of La_2O_3 Doping on the Electrical Properties of 0.5$Ba_{0.8}Ca_{0.2}TiO_3$-0.5$BaTi_{0.8}Sn_{0.2}O_3$-0.02Pr_6O_{11} Lead-Free Ceramics. *J. Phys. Chem. Solids* **2022**, *160*, 110366. [CrossRef]
34. Mahmoud, A.E.R.; Babeer, A.M. Intrinsic and Extrinsic Contributions in Nonlinear Dielectric Response of ($Bi_{0.5}Na_{0.3}K_{0.2}$)TiO_3-($Ba_{0.8}Ca_{0.2}$)TiO_3-Based $SrTiO_3$ Ceramics Driven by the Rayleigh Model. *J. Electron. Mater.* **2022**, *51*, 378–390. [CrossRef]
35. Shen, Z.; Liu, H.; Shen, Y.; Hu, J.; Chen, L.; Nan, C. Machine Learning in Energy Storage Materials. *Interdiscip. Mater.* **2022**, *1*, 175–195. [CrossRef]
36. Wang, C.; Shi, P. $Bi_{0.2}Sr_{0.7}TiO_3$–Doped $Bi_{0.5}Na_{0.5}TiO_3$–Based Lead-Free Ceramics with Good Energy Storage Properties. *J. Mater. Sci. Mater. Electron.* **2023**, *34*, 1774. [CrossRef]
37. Zhao, H.; Yu, X.Y.; Guo, Q.; Yang, H.; Li, F.; Zhang, S.; Wu, X. Large Piezoelectricity and High Depolarization Temperature in $BiScO_3$-$BiYbO_3$-$PbTiO_3$ Ceramics for Energy Harvesting at Elevated Temperatures. *J. Mater. Chem. C* **2023**, *11*, 16536–16544. [CrossRef]
38. Wang, H.; Yuan, H.; Hu, Q.; Wu, K.; Zheng, Q.; Lin, D. Exploring the High-Performance (1 − x)$BaTiO_3$-x$CaZrO_3$ Piezoceramics with Multiphase Coexistence (R-O-T) from Internal Lattice Distortion and Domain Features. *J. Alloy. Compd.* **2021**, *853*, 157167. [CrossRef]
39. Yun, H.; Kong, D.; Aoyagi, M. Characteristics of Thickness-Vibration-Mode PZT Transducer for Acoustic Micropumps. *Sens. Actuators A Phys.* **2021**, *332*, 113206. [CrossRef]
40. Cheng, H.; Zhou, W.; Du, H.; Luo, F.; Wang, W. Microstructure and Dielectric Properties of ($K_{0.5}Na_{0.5}$)NbO_3–$Bi(Zn_{2/3}Nb_{1/3})O_3$− xmol%CeO_2 Lead-Free Ceramics for High Temperature Capacitor Applications. *J. Mater. Sci. Mater. Electron.* **2015**, *26*, 9097–9106. [CrossRef]